Quantitative Estimates of Visual Performance Features in Fossil Birds

Lars Schmitz*

Department of Geology, University of California at Davis, Davis, California 95616

ABSTRACT Eyeball structures such as the lens diameter (LD) and axial length are generally assumed to be highly correlated with optically meaningful parameters. However, these optical constraints on eyeball macroanatomy have never been tested explicitly. Tradeoffs between benefits of improved visual performance and cost of adaptation from an increase of tissue production predict that when eyeball size increases, optical parameters such as posterior nodal distance and maximum entrance pupil diameter should increase isometrically with eyeball axial length and LD, respectively. Here I show quantitatively that the interspecific allometry of the avian eye largely follows this predicted isometry. Additionally, I elaborate a method to estimate optically significant eyeball soft-tissue dimensions from scleral ring and orbit morphology based on analyses of interspecific allometry in Aves. The stringent correlations between avian eyeball morphology and optical function render this system ideal for the analysis of form–function relationships and allow for an accurate estimate of optically significant eyeball soft-tissue dimensions such as diameter, axial length, and LD in fossil species. J. Morphol. 270:759–773, 2009.

KEY WORDS: eye morphology; scleral rings; optical function; visual performance; fossil birds

INTRODUCTION

Vision has an outstanding function in many invertebrate and vertebrate species and serves several purposes in intra-and interspecific interactions (Walls, 1942; Lythgoe, 1979; Land and Nilsson, 2002). Many predatory species rely on visual cues to detect their prey items, and visual information also helps maintain group cohesion of social foragers. Vision is a primary information source for motion and navigation control needed for pursuit and capture of actively moving prey. Prey species detect and avoid predators by sight. Vision is also important in finding and selecting mates.

The shape and size of external and internal eyeball structures are expected to reflect visual characteristics of animals. Eyeball morphology is generally assumed to be matched to the physical characteristics of the animal's visual environment (Walls, 1942; Lythgoe, 1979; Land and Nilsson, 2002), which would render the eye ideal for the study of its form–function relationships. Such a study could also establish morphological traits that reflect visual performance features, which, in turn, could be used to study fossil specimens. However, neither the correlation of morphological features with optical function nor the estimate of eyeball soft-tissue dimensions based on osteology has been tested explicitly.

Physiological optics predicts two main optical determinants of visual performance: the posterior nodal distance (PND) and the diameter of the maximum entrance pupil (see Fig. 1). Visual performance is characterized by two main qualities: acuity and light sensitivity. Acuity, usually given as spatial sampling frequency, expresses the fineness of detail that can be discriminated (Land, 1981). Spatial sampling frequency depends on two variables. The first variable, PND, equals the distance from the posterior nodal point to the retinal surface (see Fig. 1). The posterior nodal point is defined by the intersection of straight lines connecting points on the image on the retina to equivalent points on the imaged objects, accounting for all refractive surfaces in the optical system. The second variable is the average distance between adjacent retinal receptor cells (s), assuming a dense hexagonal packing of photoreceptor cells.

0.01*(PND/s)

spatial sampling frequency

$$v_s = \frac{\mathrm{PND}}{\sqrt{3} \cdot s \cdot \frac{180}{\pi}} \ [\mathrm{cycles/deg}] \quad (\mathrm{Miller}, 1979), \quad (1)$$

Because visual performance is an integrated result of various steps in the visual process (Hung and Ciuffreda, 2002), including the optical and neurological (retina and brain) system, one needs to test whether the anatomical modeling matches behavioral measurements. Behavioral measure-

Contract grant sponsor: DAAD (Doctoral stipend, German Academic Exchange Service).

*Correspondence to: Lars Schmitz, Department of Geology, University of California at Davis, Davis, CA 95616.
E-mail: lschmitz@ucdavis.edu

Received 18 May 2008; Revised 30 October 2008;
Accepted 7 November 2008

Published online 2 January 2009 in
Wiley InterScience (www.interscience.wiley.com)
DOI: 10.1002/jmor.10720

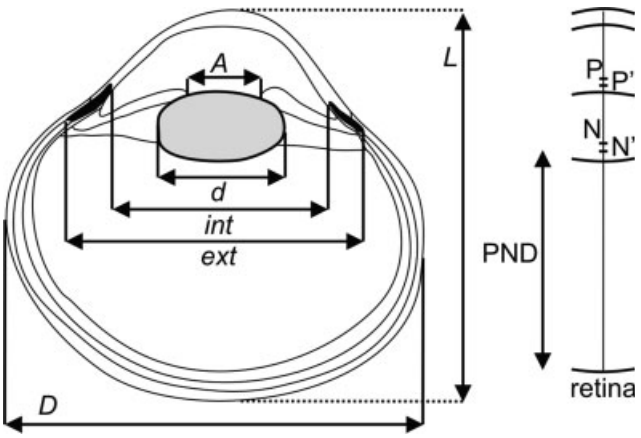

Fig. 1. Simplified crosssection of an avian eyeball with anatomical dimensions and optical parameters. A, aperture; d, equatorial lens diameter; D, eyeball diameter; ext, external scleral ring diameter; int, internal scleral ring diameter; L, eyeball axial length; N, anterior nodal point; N′, posterior nodal point; P, anterior principal point; P′, posterior principal point; PND, posterior nodal distance.

ments of acuity usually rely on repeated two-choice discrimination tasks, which help to determine the smallest resolvable visual angle. Kiltie (2000) found that values between anatomically modeled and behaviorally determined visual acuity agreed well.

The second quality of visual performance, light sensitivity, describes the brightness of the image and indicates how well an optical system functions in various light environments, especially dim light. Light sensitivity to an extended scene with broad light wave spectrum, i.e., typical of terrestrial habitats, can be modeled as:

$$\text{sensitivity}\, S = \left(\frac{\pi}{4}\right)^2 A^2 \left(\frac{d}{\text{PND}}\right)^2 \left(\frac{k \cdot l}{2.3 + k \cdot l}\right) \quad \text{(Land, 1981)}, \quad (2)$$

where d is the diameter of retinal photoreceptors (rods and cones), l photoreceptor length, and k the peak absorption coefficient of the visual pigment. A is the diameter of aperture, i.e., the diameter of the pupil (see Fig. 1). The brightness of the image that is projected onto the retina is proportional to

$$\left(\frac{A}{\text{PND}}\right)^2, \quad (3)$$

the square of the inverse f-number commonly used in optics (Land, 1981; Martin, 1982, 1983). Given everything else remains constant, the eye with a lower f-number is expected to have better light sensitivity, and this is relatively well supported by behavioral measurements of the absolute visual threshold (Martin, 1982). The absolute visual threshold describes the minimum amount of photons that can be detected with more than 50% reliability. Sensitivity to point-like light sources such as stars in moonless nights or bioluminescent light flashes largely depends on the size of the aperture A (Land, 1981; Warrant, 2004):

$$N \sim \frac{E \cdot A^2}{16 r^2}, \quad (4)$$

where N is the number of photons received by a photoreceptor, E is the number of photons originating at the light source, and r the distance from source to receptor in meters.

Visual light sensitivity is also affected by the absolute number of photoreceptors. A large number of photoreceptors lower the visual threshold by improving the signal to noise ratio. The number of photoreceptors is expected to increase with the square of eyeball diameter (∼retinal area), whereas the number of thermally induced false signals ("dark noise") scales with the square root of the number of photoreceptors (Barlow, 1988). Hence, an eyeball with large diameter is usually more light sensitive.

This study evaluates if macroanatomical eyeball dimensions, specifically axial length and equatorial lens diameter (LD) of the vertebrate eye are highly correlated with visual performance features such as PND and pupil diameter, based on original measurements of mainly Mammalia and Aves, supplemented by data on Squamata, Anura, and Teleostei. Both eyeball axial length and equatorial LD have been used to estimate PND and the diameter of the maximum entrance pupil, respectively (e.g., Hughes, 1977; Motani et al., 1999); however, it has not been explicitly tested if these morphological features are indeed highly correlated with optical parameters. This work assumes that an eye with larger diameter has a larger retina area that can contain more photoreceptors (Motani et al., 1999). Second, I explore eyeball dimensions (diameter, axial length, and LD) of extant Aves to determine correlation of osteological dimensions, i.e., scleral ring and orbit morphology. If eyeball soft-tissue dimensions are highly correlated to osteological features, it is possible to quantitatively estimate eyeball morphology in fossil Aves. Such knowledge would be valuable for the study of the evolution of visual characteristics using the fossil record.

MATERIALS AND METHODS

Testing Isometry of Morphological and Visual Performance Features

Physiological optics predicts that visual performance scales isometrically with PND and the diameter of the maximum entrance pupil. For example, acuity scales in linear proportion to PND for a given average photoreceptor diameter (Eq. 1), i.e., better visual acuity is achieved by increasing PND. The first

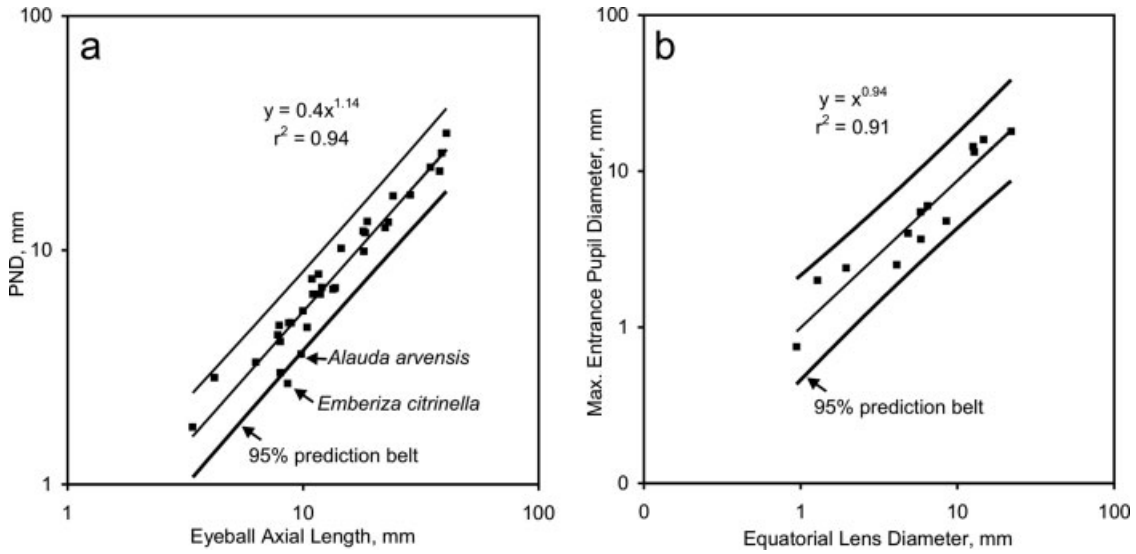

Fig. 2. **a**: Posterior nodal distance (PND) as function of eyeball axial length. **b**: Maximum entrance pupil diameter as function of equatorial lens diameter. Regression statistics are based on OLS.

step to improve visual acuity is to maximize PND for a given eyeball axial length, which maximizes the benefit from a given metabolic investment. The narrow range of the ratio of PND to eyeball axial length observed in vertebrates supports this assumption (Fig. 2a). A further improvement of acuity would require an increase of eyeball axial length, which is metabolically expensive, because it requires more tissues. According to this model, we expect axial length to be increased in proportion to PND, which maintains optical function and simultaneously avoids overinvestment in either component. This predicted isometry is in contrast with the strongly negative interspecific allometry of eyeball components with body size observed in all vertebrate clades (Howland et al., 2004).

Similarly, equatorial LD is expected to scale isometrically with the diameter of the maximum entrance pupil. Light sensitivity to an extended scene scales in linear proportion to dilated pupil area (square of pupil diameter) for given photoreceptor dimensions and PND (Eqs. 2 and 3). First, we assume that every LD is maximized for a given pupil diameter. A further increase of light sensitivity would require a larger pupil and LD, which are expected to scale in proportion. Positive allometry of lens to dilated pupil diameter results in overinvestment in a morphological structure not needed for optical function.

A test of interspecific isometry can be performed using linear regression analysis [Model I, ordinary least square (OLS) regression, and Model II, reduced major axis (RMA) regression]. Dimension Y scales isometrically with dimension X, if the exponent b of the allometric equation $Y = a*X^b$ equals 1.0. It is impossible to reject the hypothesis of isometry of Y and X if b is not significantly different from 1.0. I tested this with a two-tailed t test. All calculations for the regression analyses (OLS and RMA) and t test were performed in the computer software MathCad, following procedures outlined and Sokal and Rohlf (1995).

Eyeball axial length has been used previously to estimate PND (e.g., Hughes, 1977); however, with the exception of Kiltie (2000), allometric scaling was not considered. The correlation between A and LD has largely been unexplored in the literature. The real pupil in the amniote eye is positioned between the cornea and lens. The apparent pupil when looking at an eye (entrance pupil) is slightly magnified by the refractive surface of the cornea. Similarly, there is an exit pupil, the image of the real pupil formed by the refractive surface of the lens. For many comparative optical analyses, it is sufficient to work with the diameter of the maximum entrance pupil, which can be determined with high speed flash photographs (Martin, 1983). A previous estimate gives the diameter of the fully dilated pupil as 90% of LD (Hughes, 1977). However, no data were provided to corroborate this statement, and possible allometric scaling was not considered.

I collected data on PND, maximum entrance pupil diameter, eyeball axial length, and equatorial LD from published schematic eyes; GR Martin (personal communication, 2007) provided additional measurements (Tables 1 and 2).

Estimating Eyeball Soft-Tissue Dimensions From Scleral Ring and Orbit Morphology

Eyeball and lens diameter estimated by scleral ring dimensions. Scleral ossifications offer a great possibility to estimate eyeball soft-tissue dimensions. Scleral ossicles are widespread among vertebrates and are secondarily lost only in Serpentes, Mammalia, Crocodylia, and extant Amphibia (Edinger, 1929; Franz-Odendaal and Hall, 2006). Teleostei develop up to four scleral ossicles from endochondral or perichondral ossification in the equatorial part of the eyeball. In contrast, Aves (i.e., domestic chicken, *Gallus gallus*) and Testudines (i.e., Snapping Turtle, *Chelydra serpentine*) develop scleral ossicles intramembranously from scleral mesenchyme (Franz-Odendaal, 2006; but see Andrews, 1996). Whereas the number of ossicles greatly varies among non-teleosts, ranging from four in Arthrodira to ~28 to 32 (Edinger, 1929; Franz-Odendaal and Hall, 2006) in basal Sarcopterygia, their position at the limbus, the cornea–sclera junction, remains constant. The ossicles form an imbricate ring (scleral ring) that encloses an elliptical to circular opening (Fig. 5f,g). Motani et al. (1999) used the external scleral ring diameter to estimate eyeball diameter in Ichthyosauria. However, this clade might be unique in having scleral rings that cover more than a hemisphere of the eyeball, judging from the lateral curvature of three-dimensionally preserved rings. Motani et al. (1999) also estimated equatorial LD from the internal scleral ring diameter for lepidosaurs; however, it has not been studied if this proportion changes with increasing eyeball size.

Eyeball diameter and axial length estimated by orbit dimensions. The amniote eye is contained within the orbit

TABLE 1. Axial length and PND

	Common name	Class	Order	*L* (mm)	PND (mm)	DAP, LS	Reference
Alauda arvensis	Skylark	Av	Passeriformes	9.8	3.6	d	Donner, 1951
Aquila audax	Wedge-tailed Eagle	Av	Falconiformes	34.7	22.6	d	Reymond, 1985
Bubo virginianus	Great horned Owl	Av	Strigiformes	38.7	26.0	c	Murphy et al., 1985
Callithrix jacchus	Common Marmoset	M	Primates	10.9	7.6	d	Troilo et al., 1993
Carassius auratus	Goldfish	Ac	Cypriniformes	4.2	2.9	aq	Hughes, 1977
Columba livia	Common Pigeon	Av	Columbiformes	11.6	7.9	d	Hughes, 1977
Didelphis marsupialis	Common Opossum	M	Didelphimorphia	10.0	5.5	n	Oswaldo-Cruz et al., 1979
Emberiza citrinella	Yellowhammer	Av	Passeriformes	8.6	2.7	d	Donner, 1951
Emberiza schoeniclus	Reed Bunting	Av	Passeriformes	8.0	3.0	d	Donner, 1951
Equus caballus	Horse	M	Perissodactyla	40.6	31.6	c	Sivak and Allen, 1975
Erithacus rubeculus	English Robin	Av	Passeriformes	10.4	4.7	d	Donner, 1951
Falco berigora	Brown Falcon	Av	Falconiformes	23.0	13.2	c	Reymond, 1987
Felis domesticus	Cat	M	Carnivora	22.3	12.5	c	Hughes, 1977
Fringilla coelebs	Chaffinch	Av	Passeriformes	8.9	4.9	d	Donner, 1951
Gekko gekko	Tokay Gecko	R	Squamata	11.0	6.5	n	Hughes, 1977
Homo sapiens	Man	M	Primates	24.1	17.1	d	Hughes, 1977
Iguana iguana	Green Iguana	R	Squamata	8.7	4.9	d	Hughes, 1977
Macaca fasciularis	Long-Tailed Macaque	M	Primates	18.4	11.9	d	Lapuerta and Schein, 1995
Macaca mulatta	Rhesus Monkey	M	Primates	18.0	12.1	d	Pettigrew et al., 1988
Mus musculus	House Mouse	M	Rodentia	3.4	1.8	n	Remtulla and Hallet, 1985
Oryctolagus cuniculus	European Rabbit	M	Lagomorpha	18.1	9.9	n	Hughes, 1977
Pteropus giganteus	Indian Flying Fox	M	Chiroptera	12.0	6.9	n	Neuweiler, 1962
Puffinus puffinus	Manx Shearwater	Av	Procellariiformes	11.8	6.5	aq	Martin and Brooke, 1991
Rana esculenta	Common Water Frog	Am	Anura	8.0	4.1	n	Hughes, 1977
Rattus norvegicus	Norway Rat	M	Rodentia	6.3	3.3	n	Hughes, 1977
Saimiri sciureus	Squirrlel Monkey	M	Primates	14.5	10.2	d	Cowey and Ellis, 1967
Spheniscus humboldti	Humboldt Penguin	Av	Sphenisciformes	18.7	13.3	aq	Martin and Young, 1984
Strix aluco	Tawny Owl	Av	Strigiformes	28.5	17.2	c	Martin, 1982
Struthio camelus	Ostrich	Av	Struthioniformes	38.0	21.8	c	Martin et al., 2001
Sturnus vulgaris	European Starling	Av	Passeriformes	7.9	4.8	d	Martin, 1986
Tupaia belangeri	Tree Shrew	M	Scandentia	7.8	4.4	d	Norton and McBrien, 1992
Turdus merula	Common Blackbird	Av	Passeriformes	13.4	6.8	d	Donner, 1951
Turdus pilaris	Fieldfare	Av	Passeriformes	13.7	6.9	d	Donner, 1951

Ac, Actinopterygii; Am, Amphibia; aq, aquatic; Av, Aves; c, cathemeral and crepuscular; DAP, diel activity pattern; d, diurnal; L, axial eyeball length; LS, lifestyle; M, Mammalia; n, nocturnal; PND, posterior nodal distance; R, Reptilia. Data on DAP and LS were taken from references given above and complemented using Glutz von Blotzheim (1987–1997), Estes (1991), König et al. (1999), Nowak (1999), and Davies (2002).

cavity, the so-called "eye socket." A qualitative assessment suggests that overall eyeball dimensions are better inferred by orbit structure in clades with large eyes with respect to body and/or skull size. Birds have absolutely and relatively large eyeballs (i.e., axial length, Howland et al., 2004), only matched by primates among extant amniotes, and thus, it is expected that overall eyeball dimensions (axial length, diameter) are faithfully represented by orbit structure (orbit length, orbit depth).

Prediction intervals vs. confidence intervals. As stated earlier, my work pursues the development of a method for estimating visual characteristics from scleral ring and orbit morphology. Such estimates are made based on a log-linear regression equation (Model I) derived from empirical data, where the desired dimension is given by the allometric equation $Y = a^*X^b$. The 95% confidence interval (CI) describes a range around the expected mean Y that contains 95% of the sample means (Sokal

TABLE 2. Lens and maximum pupil entrance diameter

	Common name	Class	Order	Lens Ø (mm)	*A* (mm)	References
Carollia perspicillata	Short-Tailed Bat	M	Chiroptera	1.28	2.00	Suthers and Wallis, 1970
Didelphis marsupialis	Common Opossum	M	Didelphimorphia	6.44	6.00	Oswaldo-Cruz et al., 1979
Felis domesticus	Cat	M	Carnivora	12.60	14.40	Vakkur and Bishop, 1963
Myotis sodalis	Indiana Bat	M	Chiroptera	0.94	0.75	Suthers and Wallis, 1970
Phyllostomus hastatus	Spear-Nosed Bat	M	Chiroptera	1.95	2.40	Suthers and Wallis, 1970
Pteropus giganteus	Indian Flying Fox	M	Chiroptera	8.50	4.80	Neuweiler, 1962
Puffinus puffinus	Manx Shearwater	Av	Procellariiformes	5.84	3.67	Martin and Brooke, 1991
Rana esculenta	Common Water Frog	Am	Anura	4.84	4.00	DuPont and Degroot, 1976
Spheniscus humboldti	Humboldt Penguin	Av	Sphenisciformes	5.81	5.49	Martin and Young, 1984
Strix aluco	Tawny Owl	Av	Strigiformes	12.80	13.30	Martin, 1982
Struthio camelus	Ostrich	Av	Struthioniformes	14.68	15.96	pers. comm. GR Martin
Sturnus vulgaris	Common Starling	Av	Passeriformes	4.10	2.51	Martin, 1986
Balaenoptera physalus	Fin Whale	M	Cetacea	22.00	18.00	Pilleri and Wandeler, 1964

A, maximum pupil entrance diameter; Am, Amphibia; Av, Aves; M, Mammalia.

and Rohlf, 1995). However, CI is based on the entire set of points in the studied sample. Because I aim to estimate eyeball soft-tissue dimensions from a single observation (e.g., a single scleral ring), I use prediction intervals (PIs) instead. PI describes the range around the expected mean of Y with 95% probability to contain the true mean adjusted for the new sample size (Sokal and Rohlf, 1995). PIs are usually much wider than CIs but more useful in predictions that use a single observation (Sokal and Rohlf, 1995).

Soft-tissue dimensions. I measured ocular soft-tissue dimensions from two kinds of specimens, frozen and paraffin preserved (Tables 3–5) and augmented the data from the literature. I dissected frozen bird specimens provided by the Museum for Fish and Wildlife Biology at the University of California Davis after removing all attached ocular muscles from the isolated eyeballs. I then reinflated the eyeballs with a small gauge injection needle following published procedures (Kirk, 2004), until the eye regained a globose shape and could not be inflated any further. I measured exterior dimensions (eyeball diameter, axial length; Fig. 1) with a reticule on a Leica S6D microscope. If the eyeballs exceeded 15 mm in diameter or axial length, which is the case in about 20% of the samples, I used digital calipers instead. Freezing may affect lens dimensions, whereas the strong scleral tissues of the eye cup are unlikely to show significant changes in gross dimensions.

I retrieved further data from hemisectioned eyeballs embedded in paraffin, housed in the collection of the Zoological Society of San Diego. Eyes were excised within 1 day after death of the animal and immediately fixed in Davidson's solution, transected sagittally, then processed routinely and embedded in paraffin. Davidson's solution is a mixture of 95% ethanol, distilled water, 10% formalin, and glacial acetic acid, and presumably minimizes the risk of artifactual tissue alterations. I examined the sections with a binocular microscope for accuracy of the position of hemisections, using the clear lens and the iris as point of reference. I measured equatorial lens and internal scleral ring diameter (Figs. 1 and 3d, Table 5) from digital photographs taken with a Nikon D70 with a Nikon AF Micro Nikkor 60 mm lens.

Osteological dimensions. I skeletonized frozen bird heads and excised eyeballs, using ~10% KOH solution and mechanical preparation. I used soapy water to soften tissues attached to scleral rings, and to avoid damage of the fragile and flexible ossicles I only prepared the lateral half of scleral rings. This procedure is sufficient to measure external and internal diameter and helps maintain the original shape of the scleral ring.

The anteroposterior orbit length was measured with digital calipers, as were exterior and interior diameters of scleral rings (Tables 3 and 4). The orbit depth was calculated as the perpendicular distance from the midpoint of orbit plane to the sagittal plane. Three-dimensional coordinates were collected with a Microscribe G2X (6 DOF) along the orbit rim. Selected point coordinates were used to define the least square best-fit plane. The sagittal plane was also defined by a minimum of five three-dimensional coordinates. Orbit depth was then calculated as the perpendicular distance from the orbit plane center, assumed as the midpoint of the line connecting the most anterior and posterior points of the orbit rim, to the sagittal plane. All calculations were performed in the computer software Maple (version 10).

Selection of specimens. I studied 102 bird species represented by one or more individuals (total $n = 120$) to analyze correlations between eyeball (diameter and axial length) and scleral ring dimensions (Table 3). These birds have been classified in 12 orders (Anseriformes, Caprimulgiformes, Charadriiformes, Ciconiiformes, Cuculiformes, Falconiformes, Galliformes, Gruiformes, Passeriformes, Piciformes, Procellariiformes, Struthionithiformes), representing all four major clades within Neornithes: Palaeognathae, Galloanserae, Metaves, and Coronaves (Ericson et al., 2006).

I used measurements of 22 bird species for the analysis of the correlation between LD and INT (Table 5). The 22 species belong to 12 different orders (Anseriformes, Ciconiiformes, Columbiformes, Coraciiformes, Falconiformes, Galliformes, Passeriformes, Piciformes, Psittaciformes, Rhynochetidae, Strigiformes, and Struthioniformes), again representing all four major clades within Neornithes.

The size of the analyzed avian eyeballs spans an order of magnitude, which represents almost the entire eye size variability within Aves. The smallest eye considered for this study is that of the Lesser Goldfinch (*Carduelis psaltria*), with a diameter of 5.97 mm and an axial length of 5.32 mm. The largest eye included in this work is that of the Emu (*Dromaius novaehollandiae*), with a diameter of 49 mm and an axial length of 39 mm.

Possible phylogenetic bias. Interspecific biometric datasets are often considered to contain statistically nonindependent observations because of the hierarchical nature of phylogenetic systems (Felsenstein, 1985). A solution to this potential problem in comparative analyses is the calculation of phylogenetically independent contrasts (Felsenstein, 1985); however, I did not use this method for multiple reasons. The topology and branch lengths of avian phylogenies is despite recent efforts in parts still poorly understood, with discrepancy among the latest publications (e.g. Ericson et al., 2006; Pereira and Baker, 2006; Slack et al., 2006; Hackett et al., 2008). A key variable in the calculation of phylogenetically independent contrasts is a reasonable estimate of branch length. A longer branch represents a longer process of evolutionary change over a longer period of time than a short branch. Often, the estimate of branch length is circumvented by arbitrarily setting branch length to one; however, this approach will produce erroneous results (Björklund, 1997). Furthermore, the morphology of the avian eye is virtually identical across all major clades within Aves (with the exception of owls), and importantly, the main features of the eye seem largely optically constrained. Hence, the phylogenetic bias should be minimal.

Institutional Abbreviations

SD, San Diego Zoo; WFB, Museum for Fish and Wildlife Biology, University of California, Davis.

RESULTS

Testing Isometry of Morphological and Visual Performance Features

PND and eyeball axial length. PND is correlated with eyeball axial length ($r^2 = 0.97$), based on values obtained from the literature on 33 vertebrate species (Table 1). A log–log plot of PND versus axial length (Fig. 2a) reveals slightly positive allometry of PND. The allometric slope (OLS slope = 1.14, 95% CI = 1.02–1.24; RMA slope = 1.17, CI = 1.06–1.28; consult Table 6 for a summary of regression statistics) is similar to that found by Kiltie (2000). Both OLS and RMA slope are different from 1.0 ($p_{OLS} = 0.02$, $p_{RMA} < 0.001$). A linear regression on the raw data with a forced intercept of zero yields PND = 0.64*axial length ($r^2 = 0.95$). This confirms previously reported values (Hughes, 1977; Murphy and Howland, 1987). An eyeball with an axial length of 10 mm is predicted to have a minimum PND (= lower 95% prediction belt of OLS regression) of 3.92 mm and a maximum PND (= upper 95% prediction belt of OLS regression) of 10.34 mm, with an expected PND of 6.37 mm. Only two published PND measurement (*Emberiza citronella* and *Alauda arvensis*, both published by

TABLE 3. Scleral ring and eyeball dimensionsof birds

	Common name	Order	Coll. no. WFB	*D* (mm)	*L* (mm)	EXT (mm)
Accipiter striatus	Sharp-shinned Hawk	Falconiformes	7384, B84	15.32	14.27	12.90
Aegolius acadicus	Northern Saw-Whet Owl	Strigiformes	B110	16.74	15.22	16.72
Ammodramus caudacutus	Saltmarsh Sharp-tailed Sparrow	Passeriformes	6512, 6513	7.42	6.94	5.81
Ammodramus maritimus	Seaside Sparrow	Passeriformes	6394, 6395	10.16	8.06	6.29
Amphispiza belli	Sage Sparrow	Passeriformes	6098	8.23	7.42	6.29
Anas bahamensis	White-Cheeked Pintail	Anseriformes	6030	14.52	12.90	11.77
Anas discors	Blue-winged Teal	Anseriformes	6008	13.06	11.77	11.29
Anas platyrhynchos	Mallard, Hawaiian Hybrid	Anseriformes	6025	15.32	13.23	12.90
Anas wyvilliana	Hawaiian Duck	Anseriformes	5887, 5888	14.84	13.23	11.69
Aphelocoma californica	Western Scrub-Jay	Passeriformes	6220, B83, 116	14.78	13.23	11.08
Baeolophus bicolor	Tufted Titmouse	Passeriformes	5994	8.87	8.06	6.45
Bombycilla cedrorum	Cedar Waxwing	Passeriformes	5991	9.84	9.35	7.10
Branta sandvicensis	Hawaiian Goose	Anseriformes	6459	16.59	16.43	15.65
Bubo virginianus	Great Horned Owl	Strigiformes	B86	35.79	35.04	34.86
Calidris mauri	Western Sandpiper	Charadriiformes	6605	8.55	7.74	5.65
Caprimulgus carolinensis	Chuck-will's-widow	Caprimulgiformes	6338	18.43	12.66	17.68
Caracara cheriway	Crested Caracara	Falconiformes	6673	24.05	20.83	19.77
Carduelis psaltria	Lesser Goldfinch	Passeriformes	7411	5.97	5.32	4.03
Carpodacus purpureus	Purple Finch	Passeriformes	B62	8.06	7.58	5.81
Catharus guttatus	Hermit Thrush	Passeriformes	6224, B115	11.29	10.24	8.39
Catharus ustulatus	Swainson's Thrush	Passeriformes	6225, B117	11.05	10.00	7.90
Catoptrophorus semipalmatus	Willet	Charadriiformes	6336, 7351	14.44	12.74	10.97
Cepphus columba	Pigeon Guillemot	Charadriiformes	B54	16.13	NA	13.39
Chamaea fasciata	Wrentit	Passeriformes	6082	8.87	8.55	6.61
Charadrius vociferus	Killdeer	Charadriiformes	6191	14.52	12.42	11.45
Chondestes grammacus	Lark Sparrow	Passeriformes	6099	9.35	9.35	7.74
Cinclus mexicanus	American Dipper	Passeriformes	6105	10.48	NA	7.42
Coccyzus americanus	Yellow-billed Cuckoo	Cuculiformes	6121	13.23	12.10	10.48
Colaptes auratus	Northern Flicker	Piciformes	6307	13.71	12.26	13.39
Colinus virginianus	Northern Bobwhite	Galliformes	6252	12.90	11.45	NA
Contopus virens	Eastern Wood-Pewee	Passeriformes	6228	8.71	8.23	6.94
Cyanocitta cristata	Blue Jay	Passeriformes	6004	14.84	NA	10.48
Cygnus olor	Mute Swan	Anseriformes	6334	22.10	19.90	17.87
Dendroica caerulescens	Black-throated Blue Warbler	Passeriformes	6358	7.58	7.26	6.13
Dendroica coronata	Yellow-rumped Warbler	Passeriformes	5964, 6361, 6362	8.01	7.31	5.86
Dendroica fusca	Blackburnian Warbler	Passeriformes	6302	7.26	6.94	4.84
Dendroica nigrescens	Black-throated Gray Warbler	Passeriformes	6058	7.42	6.94	NA
Dromaius novaehollandiae	Emu	Sruthiorniformes	B85	49.00	39.00	34.86
Dryocopus pileatus	Pileated Woodpecker	Piciformes	6310	15.81	14.68	14.68
Dumetella carolinensis	Gray Catbird	Passeriformes	6274	11.13	10.00	8.06
Empidonax difficilis	Pacific-slope Flycatcher	Passeriformes	6159	8.87	7.90	6.61
Eudocimus albus	White Ibis	Ciconiiformes	6248	16.45	14.19	13.71
Gavia pacifica	Pacific Loon	Gaviiformes	B81	20.38	NA	16.24
Himantopus mexicanus	Black-necked Stilt	Charadriiformes	6544, 7360	15.89	14.52	12.98
Hylocichla mustelina	Wood Thrush	Passeriformes	6226	12.10	10.81	NA
Icterus bullockii	Bullock's Oriole	Passeriformes	6050	9.68	9.19	7.26
Icterus spurius	Orchard Oriole	Passeriformes	6598	8.87	7.90	6.94
Junco hyemalis	Dark-eyed Junco	Passeriformes	7142	8.87	8.06	6.29
Lanius ludovicianus	Loggerhead Shrike	Passeriformes	6079	13.87	11.94	10.32
Larus atricilla	Laughing Gull	Charadriiformes	6421	16.40	14.70	12.74
Loxia curvirostra	Red Crossbill	Passeriformes	6047	8.55	7.66	6.21
Loxia leucoptera	White-winged Crossbill	Passeriformes	6055	7.26	6.45	5.48
Melanerpes formicivorus	Acorn Woodpecker	Piciformes	6604	12.58	11.61	NA
Melanitta fusca	White-Winged Scoter	Anseriformes	B78	16.02	13.71	13.39
Melanitta perspicillata	Surf Scoter	Anseriformes	B60	16.13	14.35	12.90
Melospiza melodia	Song Sparrow	Passeriformes	5963, 6500	9.03	8.31	6.53
Nucifraga columbiana	Clark's Nutcracker	Passeriformes	6104	15.97	14.03	12.10
Nycticorax nycticorax	Black-crowned Night-Heron	Ciconiiformes	6553	24.72	19.64	20.00
Oreoscoptes montarius	Sage Thrasher	Passeriformes	6108	12.10	11.13	8.87
Passer domesticus	House Sparrow	Passeriformes	5967, 5970	8.39	7.66	6.21
Passerella iliaca	Fox Sparrow	Passeriformes	6102, B68	9.60	8.39	7.58
Petrochelidon pyrrhonata	Cliff Swallow	Passeriformes	6575	10.16	9.35	7.26
Phalacrocorax auritus	Double-Crested Cormorant	Pelecaniformes	B72	17.80	11.15	14.19
Phalacrocorax penicillatus	Brandt's Cormorant	Pelecaniformes	B88	26.16	21.47	23.27
Phalaropus fulicarius	Red Phalarope	Charadriiformes	B119	9.52	8.23	5.81
Pica nuttalli	Yellow-billed Magpie	Passeriformes	6396, B82	16.13	14.27	12.18
Picoides arcticus	Black-backed Woodpecker	Piciformes	6309	10.97	9.68	8.06

TABLE 3. (Continued)

	Common name	Order	Coll. no. WFB	*D* (mm)	*L* (mm)	EXT (mm)
Picoides pubescens	Downy Woodpecker	Piciformes	6150	9.03	7.42	6.77
Pipilo chlorurus	Green-Tailed Towhee	Passeriformes	6556	9.68	8.87	7.10
Pipilo crissalis	California Towhee	Passeriformes	6919	11.29	9.84	7.42
Pipilo erythrophtalmus	Eastern Towhee	Passeriformes	6555	11.13	9.68	8.06
Pipilo maculatus	Spotted Towhee	Passeriformes	6402, B111	10.89	10.32	7.58
Piranga ludoviciana	Western Tanager	Passeriformes	6644	10.16	9.35	7.66
Pluviolis fulea	Pacific Golden Plover	Charadriiformes	6128	16.13	14.19	12.26
Poecile atricapilla	Black-capped Chickadee	Passeriformes	7189	8.55	6.77	5.48
Polioptila caerulea	Blue-gray Gnatcatcher	Passeriformes	6258	6.45	6.13	4.84
Pooectes grammineus	Vesper Sparrow	Passeriformes	6511	9.19	8.55	6.45
Porphyrio martinica	Purple Gallinule	Gruiformes	6117, 6423	13.39	12.10	9.84
Puffinus gravis	Greater Shearwater	Procellariiformes	6346	18.04	14.47	14.19
Quiscalus quiscula	Common Grackle	Passeriformes	6606	12.90	12.10	9.19
Rallus longirostris	Clapper Rail	Gruiformes	6153	13.55	10.81	10.16
Regulus calendula	Ruby-Crowned Kinglet	Passeriformes	B65	7.26	6.45	4.84
Regulus satrapa	Golden-Crowned Kinglet	Passeriformes	5965	6.94	6.94	4.84
Sayornis saya	Say's Phoebe	Passeriformes	6227	10.00	9.19	6.45
Seiurus aurocapilla	Ovenbird	Passeriformes	6024	9.03	8.55	6.94
Sialia currucoides	Mountain Blue Bird	Passeriformes	6122	10.65	9.35	7.26
Sitta canadensis	Red-breasted Nuthatch	Passeriformes	6273	7.26	6.45	5.16
Sitta carolinensis	White-breasted Nuthatch	Passeriformes	6270	8.55	8.06	6.29
Somateria mollissima	Common Eider	Anseriformes	6136, 6138, 6139	17.26	14.53	14.19
Sphyrapicus ruber	Red-breasted Sapsucker	Piciformes	6610	10.32	8.87	7.26
Sphyrapicus varius	Yellow-billed Sapsucker	Piciformes	6297	10.32	8.87	7.42
Spizella passerina	Chipping Sparrow	Passeriformes	6571	6.94	6.45	5.65
Sturnella neglecta	Western Meadowlark	Passeriformes	6409	13.23	12.10	10.00
Synthliboramphus antiquus	Ancient Murrelet	Charadriiformes	B55	14.52	12.26	11.45
Tyrannus tyrannus	Eastern Kingbird	Passeriformes	6277	11.94	10.32	8.23
Uria aalge	Common Murre	Charadriiformes	B58	14.52	14.03	10.16
Vermivora celata	Orange-crowned Warbler	Passeriformes	6022	7.10	6.77	5.16
Vireo gilvus	Warbling Vireo	Passeriformes	6609	8.23	7.58	5.97
Vireo olivaceus	Red-eyed Vireo	Passeriformes	6269	9.19	8.39	7.26
Wilsonia pusilla	Wilson's Warbler	Passeriformes	B120	7.90	7.42	5.48
Zonotrichia atricapilla	Golden-crowned Sparrow	Passeriformes	5988	9.84	8.55	7.18
Zonotrichia leucophrys	White-crowned Sparrow	Passeriformes	6080	9.03	8.23	6.29

D, eyeball diameter; L, eyeball axial length; EXT, external diameter of scleral ring.

Donner, 1951) plotted below the lower 95% prediction belt.

Maximum entrance pupil (A) and lens diameter. The maximum entrance pupil diameter is correlated with LD. Schematic eye data of 13 species (Table 2) show that the former scales isometrically with the latter (OLS slope = 0.94, CI = 0.74–1.14; RMA slope = 0.99, CI = 0.79–1.19; Fig. 2b) with $r^2 = 0.91$. Neither OLS nor RMA slope is significantly different from 1.0 ($p_{OLS} = 0.54$; $p_{RMA} = 0.91$). The maximum entrance pupil diameter is given as 0.92*lens diameter, when the linear regression is forced through the origin. However, the prediction belts for this regression are wide. For a lens with a diameter of 10 mm, the expected pupil diameter is 9.22 mm (PI = 4.5–18.88 mm, based on OLS regression).

Estimating Eyeball Soft-Tissue Dimensions With Orbit and Scleral Ring Morphology

The results show that scleral ring dimensions are useful in estimating eyeball soft-tissue dimensions, such as eyeball diameter, axial length, and LD. Orbit structure is less useful than scleral rings in estimating eyeball dimensions.

Eyeball and lens diameter estimated by scleral ring dimensions. The external scleral ring diameter (see Fig. 1) approximates the eyeball diameter well. Eyeball diameter scales with negative allometry to external scleral ring diameter (OLS slope = 0.84, CI = 0.81–0.87, $p_{OLS} = 0$; RMA slope = 0.85, CI = 0.82–0.88, $p_{RMA} < 0.001$), as shown in Figure 3a (see Table 3 for measurements). The correlation is strong ($r^2 = 0.97$), and the prediction belts are narrow. A 10 mm external scleral ring diameter indicates an eyeball diameter of 12.92 mm (PI = 11.34–14.71 mm, based on OLS regression). This range is smaller than the prediction range obtained using orbit length as a proxy for eyeball diameter (see later), even after accounting for the unequal sample size by randomly drawing 25 samples and recalculating prediction belts.

The internal scleral ring diameter can be used to estimate the LD (Figs. 1, and 3d). LD scales iso-

TABLE 4. Orbit and eyeball dimensions of birds

	Common name	Order	Coll. no. WFB	Orbit		Eyeball	
				Length (mm)	Depth (mm)	D (mm)	L (mm)
Accipiter striatus	Sharp-Shinned Hawk	Falconiformes	B84	15.48	11.57	14.52	13.39
Aegolius acadicus	Northern Saw-Whet Owl	Strigiformes	B110	16.02	18.80	16.74	15.22
Aphelocoma californica	Western Scrub Jay	Passeriformes	B116, B83	15.00	13.03	14.68	13.39
Bubo virginianus	Great Horned Owl	Strigiformes	B86	32.23	23.08	35.79	35.04
Carpodacus pupureus	Purple Finch	Passeriformes	B62	10.16	6.92	8.06	7.58
Catharus guttatus	Hermit Thrush	Passeriformes	B115	11.23	7.43	11.29	10.48
Catharus ustulatus	Swainson's Thrush	Passeriformes	B117	11.65	8.56	11.29	9.84
Cepphus columba	Pigeon Guillemot	Charadriiformes	B54	20.09	18.75	16.13	16.13
Dromaius novaehollandiae	Emu	Struthioniformes	B85	63.10	56.98	49.00	39.00
Gavia pacifica	Pacific Loon	Gaviiformes	B81	23.35	14.21	20.38	NA
Melanerpes formicivorus	Acorn Woodpecker	Piciformes	B121	14.63	11.52	12.90	12.10
Melanitta fusca	White-Winged Scoter	Anseriformes	B78	20.34	13.46	16.02	13.71
Melanitta perspicillata	Surf Scoter	Anseriformes	B60	20.26	17.00	16.13	14.35
Melospiza melodia	Song Sparrow	Passeriformes	B112	9.01	5.30	8.87	8.23
Passerella iliaca	Fox Sparrow	Passeriformes	B68	8.15	10.28	9.84	8.06
Phalacrocorax auritus	Double-Crested Cormorant	Pelecaniformes	B72	18.88	12.26	17.80	11.15
Phalacrocorax penicillatus	Brandt's Cormorant	Pelecaniformes	B88	32.63	17.85	26.16	21.47
Phalaropus fulicarius	Red Phalarope	Charadriiformes	B119	8.66	2.97	9.52	8.23
Pica nuttalli	Yellow-Billed Magpie	Passeriformes	B82	18.77	13.76	15.81	13.55
Pipilo maculatus	Spotted Towhee	Passeriformes	B111	11.35	9.36	10.81	10.16
Regulus calendula	Ruby-Crowned Kinglet	Passeriformes	B65	7.70	6.16	7.26	6.45
Synthliboramphus antiquus	Ancient Murrelet	Charadriiformes	B55	16.24	12.09	14.52	12.26
Uria aalge	Common Murre	Charadriiformes	B58	14.80	26.21	14.03	14.03
Wilsonia pusilla	Wilson's Warbler	Passeriformes	B120	7.21	5.62	7.90	7.42
Zonotrichia atricapilla	Golden-Crowned Sparrow	Passeriformes	B118	9.89	13.95	9.84	8.71

D, eyeball diameter; L, eyeball axial length.

metrically (OLS slope = 0.97, CI = 0.86–1.08, p_{OLS} = 0.54; RMA slope = 1, CI = 0.89–1.11, p_{RMA} = 0.93) with internal scleral ring diameter, with an r^2 of 0.94 (Fig. 3b, Table 5). The LD can be calculated as 0.702*internal scleral ring diameter, based on the linear regression forced through the

TABLE 5. Internal scleral ring and lens diameter of birds

	Common name	Order	INT	*d*	Age			Coll. no. SD
					Years	Month	Days	
Apteryx australis mantelli	Northern Island Brown Kiwi	Struthioniformes	4.41	2.89	21	5	5	45835
Arborophila javanica	Chestnut-Bellied Partridge	Galliformes	6.31	4.3	6	7	12	38927
Ardea goliath	Goliath Heron	Ciconiiformes	13.47	9.74	10	7	8	43879
Athene cunicularia	Burrowing Owl	Strigiformes	11.45	8.22	1	4	15	48248
Buceros bicornis	Great Hornbill	Coraciiformes	11.55	7.9	26	0	14	40065
Coscoroba coscoroba	Coscoroba Swan	Anseriformes	8.75	5.86	1	11	6	39958
Dendrocygna arcuata	Wandering Whistling-Duck	Anseriformes	7.46	5.15	8	6	1	45198
Falco sparverius	American Kestrel	Falconiformes	6.36	5.93	10	3	24	46577
Gymnogyps californianus	California Condor	Falconiformes	12.6	8.09	4	4	3	45909
Henicophaps albifrons	New Guinea Bronzewing	Columbiformes	6.3	4.22	11	4	14	41682
Ketupa zeylonensis	Brown Fish Owl	Strigiformes	21.17	14.1	31	11	26	49690
Marmaronetta angustirostris	Marbled Teal	Anseriformes	5.95	4.03	4	11	14	40568
Meleagris ocellata	Ocellated Turkey	Galliformes	7.74	6.11	1	8	19	45338
Ploceus baglafecht	Bagaflecht Weaver	Passeriformes	8.78	5.42	0	0	29	41489
Polihierax semitorquatus	African Pygmy Falcon	Falconiformes	5.43	4.43	2	10	21	37317
Psitteuteles goldiei	Goldie's Lorikeet	Psittaciformes	4.17	3.15	3	7	1	41736
Pteroglossus beauharnaesii	Curl-Crested Aracari	Piciformes	8.24	5.73	11	0	26	45194
Ptilopsis granti[a]	Southern White-Faced Owl	Strigiformes	8.11	6.5	0	0	23	39087
Ptilopsis granti[a]	Southern White-Faced Owl	Strigiformes	6.85	4.53	0	0	25	39390
Rhynochetos jubatus	Kagu	Gruiformes	10.48	8.83	1	5	8	44313
Rollulus rouloul	Crested Partridge	Galliformes	5.84	4.08	1	8	11	38928
Streptopelia risoria[a]	Ringed Turtle-Dove	Columbiformes	5.93	3.81	2	1	19	40508
Streptopelia risoria[a]	Ringed Turtle-Dove	Columbiformes	5.06	3.95	9	9	17	48376
Treron vernans	Pink-Necked Green-Pigeon	Columbiformes	4.66	3.13	5	2	17	45335

INT, internal scleral ring diameter; d, equatorial lens diameter.
[a]Species averages were plotted for both *Ptilopsis granti* and *Streptopelia risoria*.

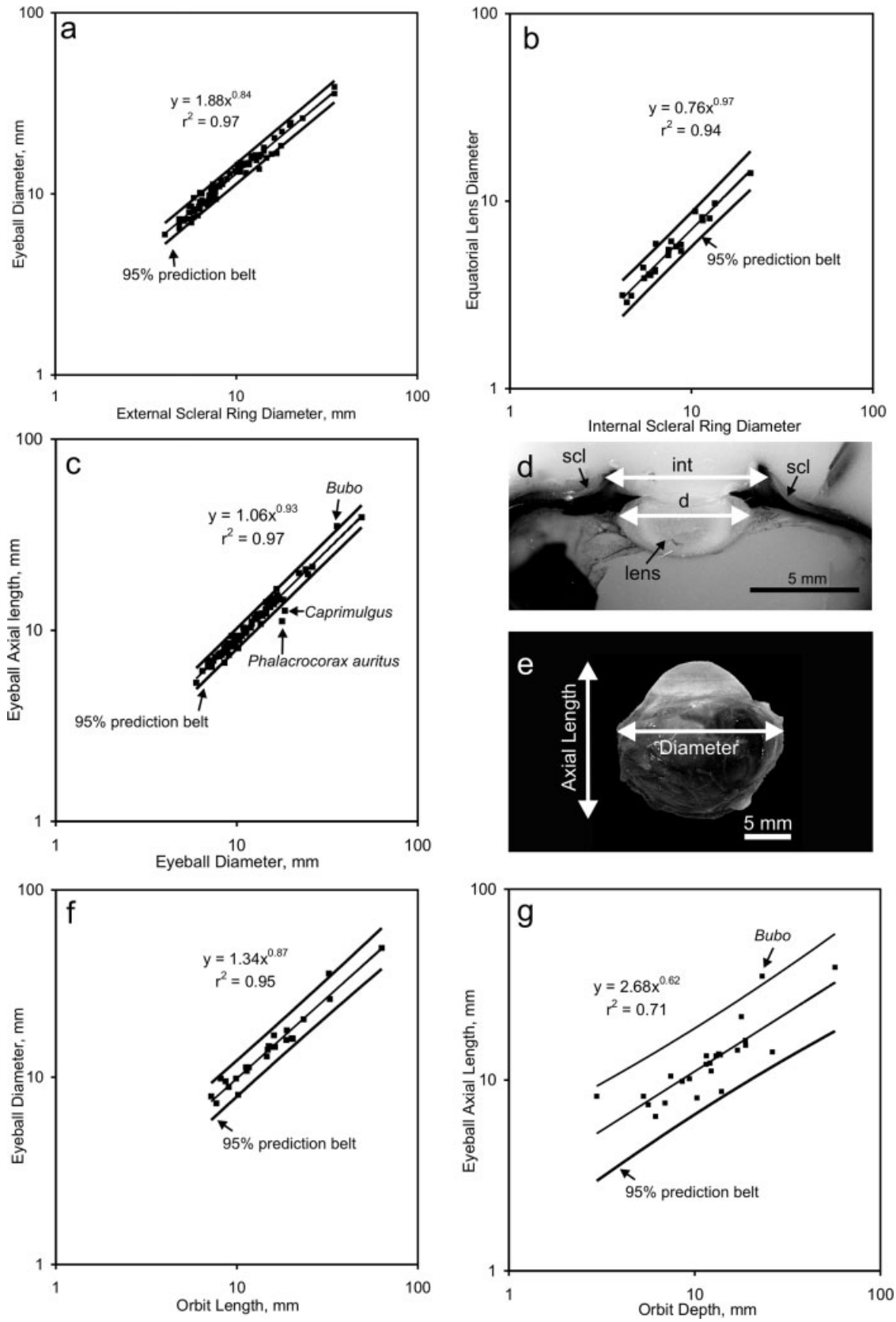

Fig. 3. Osteological correlates of eyeball morphology. **a**: Eyeball and external scleral ring diameter. **b**: Equatorial lens and internal scleral ring diameter. **c**: Eyeball axial length to eyeball diameter. **d**: Crosssection of the eye of *Meleagris ocellata* (SD 45338) illustrating measurement of equatorial lens diameter (d) and internal diameter (int) of scleral ring (scl). **e**: Side view of the eye of *Phalacrocorax auritus* (B 72) illustrating eyeball ellipticity. **f**: Eyeball diameter and orbit length. **g**: Eyeball axial length and orbit depth. Regression statistics are based on OLS.

TABLE 6. Regression statistics

	Ordinary least square			Reduced major axis		
	Slope	CI	*P*	Slope	CI	*P*
PND and axial length	1.13	1.02–1.24	0.02	1.17	1.06–1.28	<0.001
Pupil an lens diameter	0.94	0.74–1.14	0.54	0.99	0.79–1.19	0.91
Eyeball diameter and EXT	0.84	0.81–0.87	<0.001	0.85	0.82–0.88	<0.001
Lens diameter and INT	0.97	0.86–1.08	0.54	1.00	0.89–1.11	0.93
Eyeball diameter and OL	0.87	0.78–0.95	<0.001	0.89	0.80–0.98	0.01
Axial length and OD	0.62	0.44–0.79	<0.001	0.73	0.56–0.91	<0.001
Axial length and eyeball diameter	0.93	0.90–0.96	<0.001	0.94	0.91–0.98	<0.001

P values were calculated for *t* values obtained when testing for isometry.EXT, external scleral ring diameter; INT, internal scleral ring diameter; OD, orbit depth; OL, orbit length; PND, posterior nodal distance.

origin. A 10 mm internal scleral ring diameter predicts a LD of 7.02 mm (PI = 5.66–8.71 mm, based on OLS regression).

Eyeball diameter and axial length estimated by orbit dimensions. The eyeball diameter can be approximated by orbit length, measured from the most anterior to most posterior orbit margin (Fig. 3f, see Table 4 for measurements). Eyeball diameter scales slightly negatively allometric to orbit length (OLS slope = 0.87, CI = 0.78–0.95, $p_{OLS} < 0.001$; RMA slope = 0.89, CI = 0.8–0.98, $p_{RMA} = 0.01$; $r^2 = 0.95$). The prediction belts are wider than for the correlation of external scleral ring diameter with eyeball diameter. An orbit length of 10 mm predicts an eyeball diameter of 9.84 mm (PI = 7.88–12.28 mm, based on OLS regression).

Eyeball axial length can also be estimated by orbit depth (Fig. 3g, Table 4). Axial length scales negatively allometric to orbit depth (OLS slope = 0.62, CI = 0.44–0.79, $p_{OLS} < 0.001$; RMA slope = 0.73, CI = 0.56–0.91, $p_{RMA} < 0.001$). The r^2 of this regression is 0.71. The prediction belts are wide and make a faithful estimate of axial length difficult. For example, a skull with an orbit depth of 10 mm is expected to have an eyeball axial length of 11.09 mm (PI = 6.60–18.65 mm, based on OLS regression).

Axial length estimated by eyeball ellipticity. Avian eyeballs are characterized by a certain ellipticity with relatively small variance (Fig. 3e), i.e., the ratio of eyeball diameter and axial length is approximately constant, including birds of different lifestyles. Eyeball axial length scales slightly negatively allometric to eyeball diameter (OLS slope = 0.93, CI = 0.90–0.96, $p_{OLS} < 0.001$; RMA slope = 0.94, CI = 0.91–0.98, $p_{RMA} < 0.001$) as Figure 3c shows. r^2 is 0.97. Hence, it is possible to calculate axial length directly by given external scleral ring diameter: axial length = 2*(external scleral ring diameter)$^{0.78}$. As a test of the robustness of the data, I directly correlated axial length to external scleral ring diameter and obtained axial length = 1.83(external scleral ring diameter)$^{0.80}$ with $r^2 = 0.95$, which is very similar to the calculated result.

DISCUSSION

Testing Isometry of Morphological and Visual Performance Features

The analyses of the scaling of eyeball axial length with PND and LD with maximum entrance pupil diameter reveal that both anatomical features largely follow the predicted isometry. This should help maintain optical function and avoids overinvestment. Maximum entrance pupil diameter scales isometrically with LD, whereas PND scales with a slight positive allometry to axial length. Positive allometry is also found, when the data of Donner (1951), two points of which plot outside the 95% prediction belts, are removed from the regression analysis (OLS slope = 1.07, CI = 1.01–1.14, $p_{OLS} = 0.04$; RMA slope = 1.08, CI = 1.02–1.15, $p_{RMA} = 0.02$). The slight deviation from the expected isometry is surprising. A possible explanation for the positive allometry considers photoreceptor scaling as indicated by Kiltie (2000). One important assumption of my optical prediction of isometry was that the size of photoreceptors does not change with increasing eye size. If photoreceptor diameter becomes larger in eyes with longer axial length, an increase in axial length results in a relatively less improvement of visual acuity (Eq. 1). A positive allometry of PND to axial length might help overcome this effect. The scaling of visual photoreceptors in vertebrate eyes has not been studied yet; however, larger *Drosophila* eyes do have larger receptors than in smaller *Drosophila* species (Stevenson et al., 1995).

Previously, it had been suggested that diel activity pattern influences the correlation between PND and axial length. Animals can be classified as diurnal, mainly active during the day; nocturnal, active at night; crepuscular, active in twilight conditions; and cathemeral, active both day and night. Pettigrew et al. (1988) stated that nocturnal animals have a smaller ratio of PND to eyeball axial

length compared with diurnal animals. This can only be supported when removing the data of Donner (1951), which seem to be erroneous. I classified species according to their diel activity pattern (Table 2), and found that the mean of the ratio of PND to axial length for diurnal species (0.66, excluding Donner, 1951) is different from that of nocturnal species (0.55, $P < 0.001$). Similarly, the mean of the ratio of PND to axial length of crepuscular and cathemeral species (0.63) is different from that of nocturnal species ($P = 0.03$). Also, the mean of this ratio is not different between the former group and diurnal species ($P = 0.34$).

Another factor that potentially adds to the variation of PND to axial length is the preferred habitat, i.e., marine versus terrestrial. Compared with terrestrial species, aquatic vertebrates have a less steep cornea, stronger spherical lens, and an often "flattened" eye (Walls, 1942), i.e., wider equatorial diameter than axial length. One would expect to see a difference in the ratio of PND to axial length between terrestrial and aquatic species because of this fundamental difference. However, this cannot be established because of the small sample size. There are only three partially or fully aquatic species in the list of available schematic eyes, two diving birds (Manx Shearwater, *Puffinus puffinus* and Humboldt Penguin, *Spheniscus humboldti*) and the goldfish, *Carassius auratus* (Table 1).

LD is correlated with maximum entrance pupil diameter; however, this correlation is based on only 13 data points. It is necessary to obtain more measurements to further test this relationship. The main reason for the current lack of data probably is the difficulty of measuring pupil and LD. Pupil diameter should preferably be measured in live animals, because post mortem and in vivo measurements differ. For example, the maximum entrance pupil of Manx Shearwater (*Puffinus puffinus*) is 3.67 mm in vivo and 2.72 mm postmortem (Martin and Brooke, 1991). Lens biometry is very sensitive to postmortem treatment, and dimensions vary greatly depending on choice of procedures (Augusteyn et al., 2006).

Estimating Eyeball Soft-Tissue Dimensions From Scleral Ring and Orbit Morphology

The quantitative estimate of optically significant soft-tissue eyeball structures is fundamentally important for the inference of visual capacity in fossil amniotes. There are no well-preserved fossil eyeball soft tissues thus far, and hence, one is forced to use osteological structures such as the orbit cavity and the scleral ring to reconstruct soft-tissue dimensions.

Scleral rings are very useful in modeling ocular soft-tissue dimensions in birds, and therefore, some aspects of eyeball structure may be reconstructed in extinct species with scleral rings. Internal scleral ring diameter scales isometrically with LD, which indicates that this morphological feature is highly correlated with optical function. Eyeball diameter scales slightly negatively to external scleral ring diameter, i.e., the larger the scleral ring diameter the smaller the eyeball diameter relative to the ring. This indicates that in absolutely larger eyes the scleral ring is more extensively ossified, pointing to a structural constraint superimposed on the optical constraint.

The excellent correlation between scleral ring and eyeball dimensions is somewhat surprising, given the variability of scleral ring morphology in birds. The number of scleral ossicles in birds varies from 10 (Edinger, 1929) or 11 to 18 (Curtis and Miller, 1938). The lowest number occurs in doves and pigeons (Columbidae) and loons (Gaviidae), whereas the highest occurs in Anatidae and Laridae. Shape and thickness of individual scleral ossicles greatly vary (Edinger, 1929; Lemmrich, 1931; Curtis and Miller, 1938). However, together they form an imbricated ring that is usually flat with slightly concave lateral surfaces (Fig. 4f). Some Falconiformes (Fig. 4g) and especially Strigiformes (Fig. 4i) have steep sides. In the latter, the ring mimics the tubular ocular shape that is characteristic of owls.

Two aspects that I did not address in this study are intraspecific and ontogenetic variability of correlations between scleral ring and ocular dimensions, and thus one should be cautious when trying to estimate soft-tissue eyeball dimensions of juvenile fossil birds.

Dimensions of the orbit cavity are also useful to estimate avian ocular morphology, although the error margins are larger than when using scleral rings as proxy (Fig. 3g,f). The main reason for this is that the orbit rim is not well defined in some taxa. The ventral orbit margin usually features no ossified structure and is only vaguely traced by the position of the jugal arch (Fig. 4a,e; Baumel and Witmer, 1993). The shape of the dorsal orbit margin of many marine birds is influenced by salt-excreting glands, which leave deep depressions in the frontals and the orbit rim is characterized by poor ossification evidenced by multiple embayments (Fig. 4b,c). Supraorbital processes in various clades (Falconiformes, Struthioniformes without Apterygidae, Anseriformes, Strigidae, and others; compare, e.g, Mayr, 2005) further complicate the structure of the orbit rim (Fig. 4h,i). The space between the supraorbital process and frontal is filled with a membrane, and hence the lateral frontal margin is not the true orbit margin. In some birds the temporal fossa deeply notches the posterior margin of the orbit. This fossa, which traces the extension and attachment of jaw muscles, mainly the *musculi*

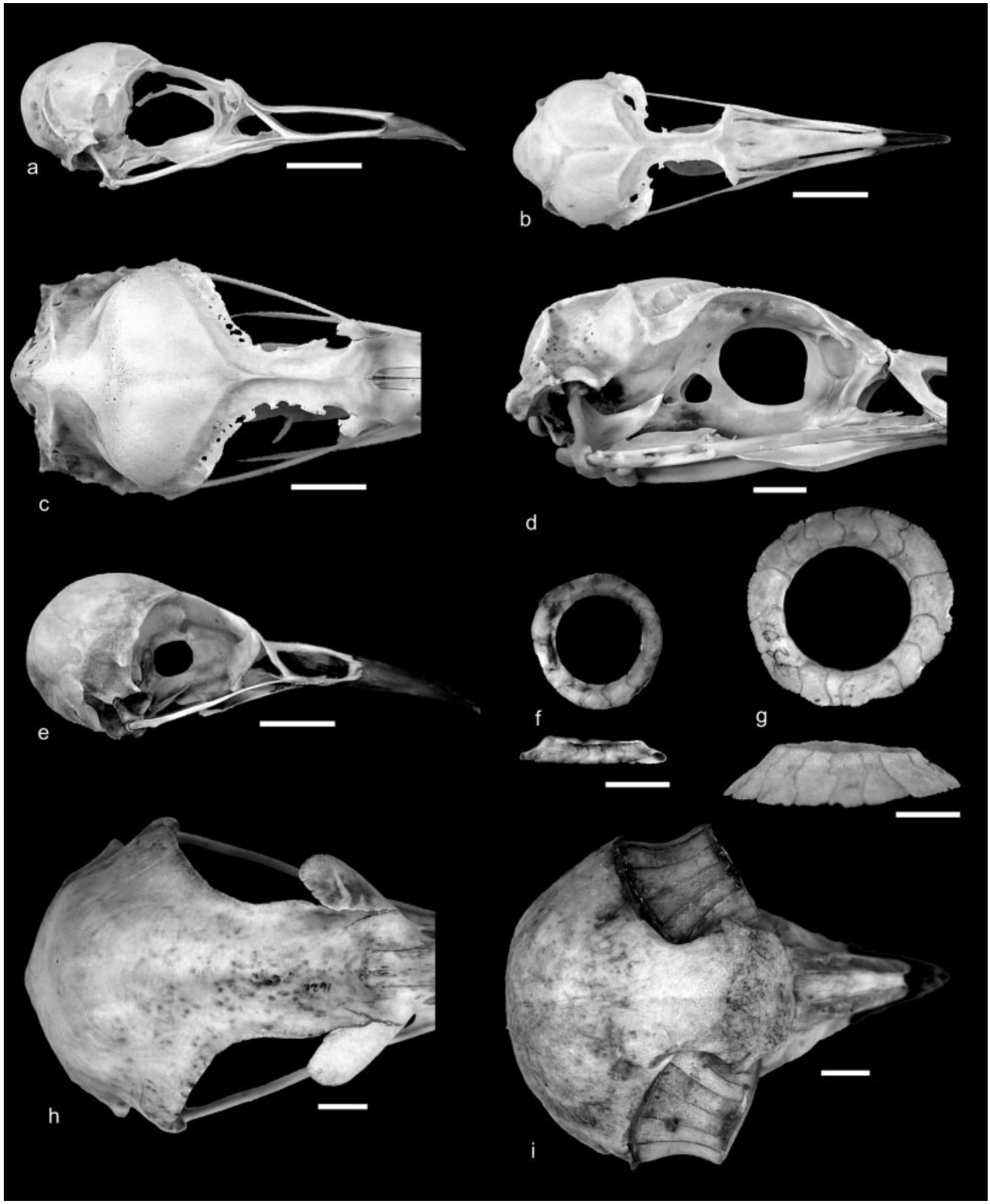

Fig. 4. Photographs illustrating orbit rim and scleral ring morphology. **a**,**b**: *Synthliboramphus antiquus* (WFB-B55). **c**: *Gavia pacifica* (WFB-B81). **d**: *Gavia immer* (WFB-B90). **e**: *Pica nuttalli* (WFB-B82). **f**: Top and side view of the scleral ring of *Phoebastria nigripes* (WFB-4827). **g**: Top and side view of the scleral ring of *Aquila chrysaethos* (WFB-1621). **h**: *Aquila chrysaethos* (WFB-1621). **i**: *Bubo virginianus* (WFB-2949). Scale bar equals 10 mm.

adductor mandibulae (Vanden Berge and Zweers, 1993), is particularly deep in, for example, herons, albatrosses, and larids (Fig. 4d). The anterior orbit margin of some birds (e.g., herons) is equally poorly defined, because the lacrimal is embayed posteriorly and at the same time the ectethmoid is largely reduced.

Difficulties in finding a good proxy for the optical axis and variability of the thickness of the sagittal wall are problematic for estimating axial length from orbit depth. I assumed that the optical axis of the eyeball was parallel to a normal of the plane defined by the orbit margin. However, the three-dimensional orientation of the plane is not well constrained when the orbit rim is poorly defined. I further assumed that eyeballs almost meet at the interorbital septum. This is true for many different clades; however, nightjars possess a thick interorbital septum and consequently I would overestimate axial length. The axial length of owls would be overestimated as well, because their eyes point anteriorly (Fig. 4i), and the normal of the orbit plane intersects the sagittal plane far posterior to the actual orbit cavity. Indeed, *Bubo virginianus* plots above the 95% prediction belt (Fig. 3g). In contrast, the owl *Aegolius acadicus* plots in the expected range.

Difficulties in estimating eyeball dimensions from orbit cavity have also been found in clades other than Aves. Among some primates, known for their relatively and absolutely large eyes with well-defined orbit rims, only some variation in orbit size relates to variation in eye size (Kirk, 2006).

SUMMARY

I demonstrate in this study that features of avian eyeball morphology are highly correlated with visual performance features. I predicted and confirmed that LD should scale isometrically with maximum entrance pupil diameter, based on tradeoffs between the benefits of optical function and the cost of tissue production. I could not confirm my second prediction, isometry between axial length and PND. PND scales with positive allometry to axial length, which can possibly be explained by changes in size of photoreceptors with increasing eye size.

Furthermore, I show that the external and internal diameter of the scleral ring of Aves are highly correlated with eyeball diameter, axial length, and LD, all of which are significant for optical function. Despite the limitations discussed earlier, eyeball dimensions may also be estimated from orbit dimensions in fossil birds, in particular when scleral rings are not fossilized. Thus, it is possible to quantitatively estimate visual performance features of fossil Aves within narrow error margins. For example, it is possible to estimate the eyeball axial length of a fossil bird, which conveys important clues about potential visual acuity. Similarly, estimates of the equatorial LD of a fossil bird can be interpreted with respect to potential light sensitivity.

Form–function relationships are an important resource for the study of structural, functional, and behavioral diversity of extant and extinct taxa. A general requirement for the study of structural adaptation is the establishment of links between structure, function, and performance (Lauder, 1990, 1995; Reilly and Wainwright, 1994). This study represents a first analysis of the relationships between the morphology, optical function, and visual performance of avian eyes. Future studies will quantitatively explore links between visual performance and ecology, for example, predator behavior or diel activity pattern, motivated by the research question if a certain morphological feature is correlated with a specific type of behavior. If this can be corroborated, we will also be able to make quantitative inferences of lifestyle and behavior in extinct taxa.

ACKNOWLEDGMENTS

Irene and Andrew Engilis (Fish and Wildlife Museum at UC Davis) and preparatory staff provided access to their collections, bird specimens, and preparation assistance. Graham Martin (University of Birmingham) provided additional schematic eye data. I thank the Zoological Society of San Diego, in particular Rebecca Papendieck and staff, for access to their collection. I am grateful to my PhD advisor Ryosuke Motani and my committee members (Sandy Carlson, Ivan Schwab, Gary Vermeij, and Peter Wainwright).

LITERATURE CITED

Andrews KD. 1996. An endochondral rather than a dermal origin for scleral ossicles in cryptodiran turtles. J Herpetol 30:257–260.

Augusteyn RC, Rosen AM, Borja D, Ziebarth NM, Parel J-M. 2006. Biometry of primate lenses during immersion in preservation media. Mol Vis 12:740–747.

Barlow HB. 1988. Vision—The thermal limit to seeing. Nature 334:296–297.

Baumel JJ, Witmer LM. 1993. Osteologia. In: Baumel JJ, King AS, Breazile JE, Evans HE, Vanden Berge JC, editors. Handbook of Avian Anatomy. Cambridge, MA: Nuttall Ornithological Club. pp 45–132.

Björklund M. 1997. Are 'comparative methods' always necessary? Oikos 80:607–612.

Citron MC, Pinto LH. 1973. Retinal image—Larger and more illuminated for a nocturnal than for a diurnal lizard. Vision Res 13:873–876.

Cowey A, Ellis CM. 1967. Cortical representation of retina in squirrel and rhesus monkeys and its relation to visual acuity. Exp Neurol 24:374–385.
Curtis EL, Miller RC. 1938. The sclerotic ring in North American birds. Auk 55:225–243.
Davies SJJF. 2002. Ratites and Tinamous. Oxford, NY: Oxford University Press. 310 p.
Donner KO. 1951. The visual acuity of some passerine birds. Acta Zool Fennica 66:1–40.
DuPont JS, Degroot PJ. 1976. Schematic dioptric apparatus for the frog's eye (*Rana esculanta*). Vision Res 16:803–810.
Edinger T. 1929. Über knöcherne Scleralringe. Zool Jahrb Anat Ontog 51:163–226.
Ericson PGP, Anderson CL, Britton T, Elzanowski A, Johansson U, Källersjö M, Ohlson JI, Parsons TJ, Zuccon D, Mayr G. 2006. Diversification of Neoaves: Integration of molecular sequence data and fossils. Biol Lett UK 2:543–547.
Estes RD. 1991. The Behavior Guide to African Mammals. Berkeley, Los Angeles, London: The University of California Press. 611 p.
Felsenstein J. 1985. Phylogenies and the comparative method. Am Nat 125:1–15.
Franz-Odendaal TA. 2006. Intramembranous ossification of scleral ossicles in *Chelydra serpentina*.. Zoology 109:75–81.
Franz-Odendaal TA, Hall BK. 2006. Skeletal elements within teleost eyes and a discussion of their homology. J Morphol 267:1326–1337.
Glutz von Blotzheim UN. 1987–1997. Handbuch der Vögel Mitteleuropas. Band 1–14, 2. Auflage. Wiesbaden: Aula-Verlag.
Hackett SJ, Kimball RT, Reddy S, Bowie RCK, Braun EL, Braun MJ, Choijnowski JL, Cox WA, Han K-L, Harshman J, Huddleston CJ, Marks BD, Miglia KJ, Moore WS, Sheldon FH, Steadman DW, Witt CC, Yuri T. 2008. A phylogenomic study of birds reveals their evolutionary history. Science 320:1763–1768.
Howland HC, Merola S, Basarab JR. 2004. The allometry and scaling of the size of vertebrate eyes. Vision Res 44:2043–2065.
Hughes A. 1977. The topography of vision in mammals of contrasting life style: Comparative optics and retinal organisation. In: Crescitelli F, editor. The Visual System in Vertebrates. Berlin, Heidelberg, NY: Springer-Verlag. pp 613–756.
Hung GK, Ciuffreda KJ. 2002. Models of the Visual System. Berlin, Heidelberg, NY: Springer-Verlag. 798 p.
Kiltie RA. 2000. Scaling of visual acuity with body size in mammals and birds. Funct Ecol 14:226–234.
Kirk EC. 2004. Comparative morphology of the eye in primates. Anat Rec Part A 281:1095–1103.
Kirk EC. 2006. Effects of activity pattern on eye size and orbital aperture size in primates. J Hum Evol 51:159–170.
König C, Weick F, Becking J-H. 1999. Owls—A Guide to the Owls of the World. Sussex: Pica Press. 462 p.
Land MF. 1981. Optics and vision in invertebrates. In: Land MF, Laughlin SB, Naessel DR, Strausfeld NJ, Waterman TH, editors. Comparative Physiology and Evolution of Vision in Invertebrates B: Invertebrate Visual Centers and Behavior I. Berlin, Heidelberg, NY: Springer-Verlag. pp 471–592.
Land MF, Nilsson,D-E. 2002. Animal Eyes. Oxford: Oxford University Press. 121 p.
Lauder GV. 1990. Functional morphology and systematics: Studying functional patterns in an historical context. Annu Rev Ecol Syst 21:314–340.
Lauder GV. 1995. On the inference of function from structure. In: Thomason J, editor. Functional Morphology in Vertebrate Palaeontology. Cambridge: Cambridge University Press. pp 1–18.
Lapuerta P, Schein SJ. 1995. A 4-surface schematic eye of the macaque monkey obtained by an optical method. Vision Res 35:2245–2254.
Lemmrich W. 1931. Der Skleralring der Vögel. Jena Z Naturw 65:513–586.
Lythgoe JN. 1979. The Ecology of Vision. Oxford: Clarendon Press. 244 p.
Marshall J, Mellerio J, Palmer DA. 1973. A schematic eye for the pigeon. Vision Res 13:2449–2453.
Martin GR. 1982. An owl's eye—Schematic optics and visual performance in *Strix aluco L.* J Comp Physiol 145:341–349.
Martin GR. 1983. Schematic eye models in vertebrates. In: Ottoson D, editor. Progress in Sensory Physiology, Vol. 4. Berlin, Heidelberg, NY: Springer-Verlag. pp 43–82.
Martin GR. 1986. The eye of a passeriform bird, the European starling (*Sturnus vulgaris*)—Eye movement amplitude, visual fields and schematic optics. J Comp Physiol A 159:545–557.
Martin GR, Brooke MD. 1991. The eye of a procellariform seabird, the manx shearwater, *Puffinus puffinus*—Visual fields and optical structure. Brain Behav Evol 37:65–78.
Martin GR, Young SR. 1984. The eye of the Humboldt penguin, Spheniscus humboldti—Visual fields and schematic optics. P Roy Soc B Biol Sci 223:197–222.
Martin GR, Ashash U, Katzir G. 2001. Ostrich ocular optics. Brain Behav Evol 58:115–120.
Mayr G. 2005. The postcranial osteology and phylogenetic position of the middle Eocene *Messelastur gratulator* Peters, 1994—A morphological link between owls (Strigiformes) and falconiform birds? J Vertebrate Paleontol 25:635–645.
Miller WH. 1979. Intraocular filters. In: Autrum H, editor. Comparative Physiology and Evolution of Vision in Invertebrates A: Invertebrate Photoreceptors. Berlin, Heidelberg, NY: Springer-Verlag. pp 69–143.
Motani R, Rothschild BM, Wahl W. 1999. Large eyeballs in diving ichthyosaurs—The huge eyes of these extinct reptiles may have been useful deep in the ocean. Nature 402:747–747.
Murphy CJ, Howland HC. 1987. The optics of comparative ophthalmoscopy. Vision Res 27:599–607.
Murphy CJ, Evans HE, Howland HC. 1985. Towards a schematic eye for the great horned owl. Forts Zool 30:703–706.
Neuweiler G. 1962. Bau und Leistung des Flughundauges (*Pteropus giganteus Brunn*). Z Vergl Physiol 46:13–56.
Norton TT, McBrien NA. 1992. Normal development of refractive state and ocular component dimensions in the tree shrew (*Tupaia belangeri*). Vision Res 32:833–842.
Nowak RM. 1999. Walker's Mammals of the World, 6th ed. London: The Johns Hopkins University Press. 1936 p.
Oswaldo-Cruz E, Hokoc JN, Sousa APB. 1979. Schematic eye for the opossum. Vision Res 19:263–278.
Pereira SL, Baker AJ. 2006. A mitogenomic timescale for birds detects variable phylogenetic rates of molecular evolution and refutes the standard molecular clock. Mol Biol Evol 23:1731–1740.
Pettigrew JD, Dreher B, Hopkins CS, McCall MJ, Brown M. 1988. Peak density and distribution of ganglion-cells in the retinae of microchiropteran bats—Implications fro visual acuity. Brain Behav Evol 32:39–56.
Pilleri G, Wandeler A. 1964. Ontogenese and funktionelle Morphologie des Auges des Finnwals Balaenoptera physalus Linnaeus (Cetacea, Mysticeti, Balaenopteridae). Acta Anat 57:1–74.
Reilly SM, Wainwright,PC. 1994. Conclusion: Ecological morphology and the power of integration. In: Wainwright PC, Reilly SM, editors. Ecological Morphology—Integrative Organismal Biology. Chicago: The University of Chicago Press. pp 339–354.
Remtulla S, Hallett PE. 1985. A schematic eye for the mouse, and comparisons with the rat. Vision Res 25:21–31.
Reymond L. 1985. Spatial visual acuity of the eagle *Aquila audax*—A behavioral, optical and anatomical investigation. Vision Res 25:1477–1491.
Reymond L. 1987. Spatial visual acuity of the falcon, *Falco berigora*—a behavioral, optical and anatomical investigation. Vision Res 27:1859–1874.
Sivak JG, Allen DB. 1975. Evaluation of the "ramp" retina of the horse eye. Vision Res 15:1353–1356.
Slack KE, Jones CM, Ando T, Harrison GL, Fordyce RE, Arnason U, Penny D. 2006. Early penguin fossils, plus mitochondrial genomes, calibrate avian evolution. Mol Biol Evol 23:1144–1155.

Sokal RR, Rohlf FJ. 1995. Biometry, 3rd ed. New York: W.H. Freeman and Company. 887 p.
Stevenson RD, Hill MF, Bryant PJ. 1995. Organ and cell allometry in Hawaiian Drosophila: How to make a big fly. P Roy Soc B Biol Sci 259:105–110.
Suthers RA, Wallis NE. 1970. Optics of the eyes of echolocating bats. Vision Res 10:1165–1173.
Troilo D, Howland HC, Judge SJ. 1993. Visual optics and retinal cone topography in the common marmoset (*Callithrix jacchus*). Vision Res 33:1301–1310.
Vakkur GJ, Bishop PO. 1963. The schematic eye in the cat. Vision Res 3:357–381.
Vanden Berge JC, Zweers GA. 1993. Myologia. In: Baumel JJ, King AS, Breazile JE, Evans HE, Vanden Berge JC, editors. Handbook of Avian Anatomy. Cambridge, MA: Nuttall Ornithological Club. pp 189–247.
Walls GL. 1942. The Vertebrate Eye and Its Adaptive Radiation. New York: Hafner Pub. Co. 785 p.
Warrant EJ. 2004. Vision in the dimmest habitats on Earth. J Comparative Physiol A 190:765–789.